25th ABCM International Congress of Mechanical Engineering
October 20-25, 2019, Uberlândia, MG, Brazil

PARAMETRIC ANALYSIS OF THE DYNAMICAL MODEL OF A VIBRATION-ASSISTED DRILLING TOOL, A VIBRO-IMPACT SYSTEM WITH MULTIPLE IMPACTS

d'Almeida E.F.V.
Department of Mechanical Engineering - Universidade Federal do Rio de Janeiro, Rio de Janeiro, Brazil

Aguiar R.R
Brazil Technology Integration Center - Schlumberger, Rio de Janeiro, Brazil

Ritto T.G.
Department of Mechanical Engineering - Universidade Federal do Rio de Janeiro, Rio de Janeiro, Brazil

Abstract. *The aim of this work is to analyze the axial nonlinear dynamics of a vibro-impact system used as a drilling tool. A parametric analysis investigates the effect that some design parameters have on the dynamic behavior of the system. Furthermore, a measure is proposed to evaluate the efficiency of the process, and used for design modifications of the current vibro-impact system. The results reveal the possibility of 85% increase in the impact force transfer when compared with the original design.*

Keywords: *vibration-assisted drilling, nonlinear dynamics, model validation, vibro-impact, contact*

1. INTRODUCTION

The main focus of this work is to analyze the axial dynamics of a vibration assisted drilling tool (VAD). This prototype was submitted to field tests in drilling environment to evaluate and characterize the tool performance. d'Almeida *et al.* (2019) proposed a lumped parameter vibro-impact model to describe the axial dynamics of a VAD. The results showed an overall good match between field data and model outputs, as the vibro-impact model is capable of capturing and reproducing the main dynamic behavior of the tool. Thus, the main objective of this work is to employ this mathematical model to perform a parametric analysis to evaluate how the design parameters (geometry, spring stiffness, excitation force) influences the dynamic behavior of the tool to propose design modifications for the current vibro-impact system.

2. MATHEMATICAL MODEL

A sketch of the analyzed system is shown in Fig. 1. There are four possible impact surfaces: the recoil spring (impact surface #1), the impact face (impact surface #2), the off-bottom shoulder (impact surface #3), and the on-bottom shoulder (impact surface #4). In this model, the external forces are divided into four categories: impact forces, bit-rock interaction force, excitation force, and fluid-structure interaction force. The equations of motion represent the axial displacement of the seven degrees of freedom model of a vibration-assisted drilling tool, as proposed by d'Almeida *et al.* (2019).

$$\mathbf{M}\ddot{\mathbf{x}}(t) + \mathbf{C}\dot{\mathbf{x}}(t) + \mathbf{K}\mathbf{x}(t) = \mathbf{f}(\mathbf{x}, \dot{\mathbf{x}}, t) \tag{1}$$

where $\mathbf{M}$ is the mass matrix, $\mathbf{C}$ is the damping matrix, $\mathbf{K}$ is the stiffness matrix. $\mathbf{f}(\mathbf{x}, \dot{\mathbf{x}}, t)$ is vector that contains the external forces, and $\mathbf{x}(t) \in \mathbb{R}^7$ is the vector with the axial displacement of the seven degrees of freedom.

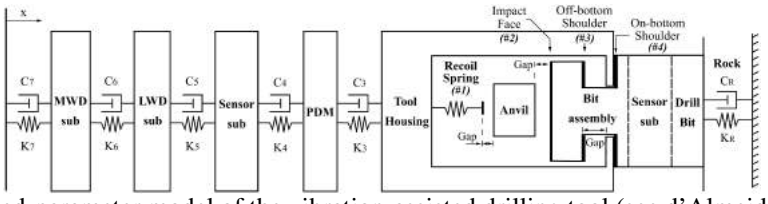

Figure 1: Lumped-parameter model of the vibration-assisted drilling tool (see d'Almeida *et al.* (2019)).

This tool is powered by an positive displacement motor (PDM), which works as an inverted positive displacement pump, converting the hydraulic power of the mud fluid into mechanical power. For modeling purposes, this means that

the excitation frequency is a function to the mud flow rate ($0.59\text{x}10^{-3}\ m^3/s$ is equal to 1 Hz). The working principle of this prototype can be summarized in five steps. First, an excitation force drives the anvil towards the bit assembly. Next, the impacting mass makes contact with the bit assembly at the impact face, which results in an impact force. After that, the excitation force pushes the anvil toward the recoil spring. In the fourth step, the anvil impacts the recoil spring, which results in deformation of the spring, which converts the kinetic energy of the impacting mass into elastic potential energy for the next cycle movement. Lastly, the spring and the excitation forces drive the impacting mass in the direction of the bit assembly, and the cycle restarts.

3. DYNAMIC BEHAVIOR

This section analyzes the acceleration data in the time domain to understand the relation between the dynamic behavior of the tool and the excitation frequency. In this analysis, the model design used the initial conditions that emulate a drilling operation, which included 155.7 kN weight on bit (static force) and an excitation frequency from 21.3 to 69.3 Hz. At a low-excitation frequency range, the axial vibration peaks indicate high-peak amplitudes and relatively low dispersion, as shown in Fig. 2a. The analysis of the axial vibration data indicates an average axial vibration peak of 64.9 g. An investigation of each impact cycle indicate that the system exhibits a periodic behavior with a regular impact frequency of 21 Hz. Next, as the excitation frequency increases, the system exhibits an increase in the maximum axial vibration peaks observed, as shown in Fig. 2b. Note that there is a significant increase in axial vibration peak dispersion, but a decrease in the average axial vibration peaks (from 64.9g to 60.3 g). The periodic behavior observed in the previous event degenerates into an aperiodic behavior. Finally, at higher excitation frequencies, there is a reduction in both axial vibration peak average (29.6g) and dispersion, as shown in Fig. 2c. The aperiodic behavior observed in the previous event returned to seemingly periodic behavior with a 27-Hz impact frequency.

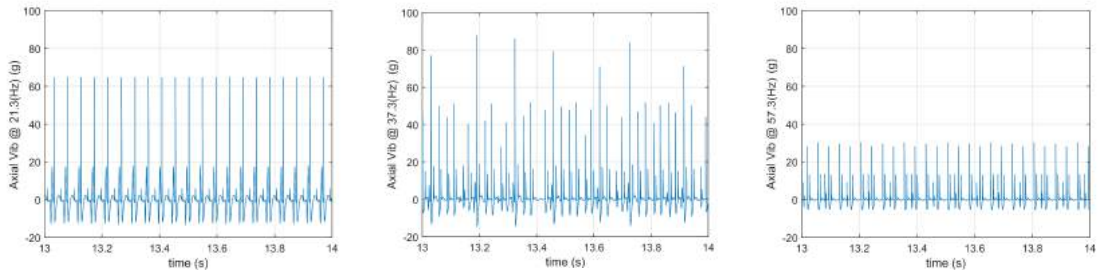

(a) (b) (c)

Figure 2: Simulation results of the axial vibration at the bit assembly obtained at constant excitation frequency at (a) 21.3 Hz, (b) 37.3 Hz, and (c) 53.3 Hz, after achieving steady-state behavior.

3.1 Classification of the dynamic behavior of the system

The classification associates the dynamic behavior observed in the simulation results with a dynamic label. This procedure requires the selection of a dynamic parameter (e.g., number of impacts in a given surface) that is affected by the change in the system's dynamic behavior. In this work, the dynamic label is defined as the number of impacts in a given surface divided by the total number of impact cycles. The definition of an impact cycle assumes that the period of this cycle coincides with the period of the excitation force. This parameter, referred to as average impacts per cycle (Z^*), simplifies the detection and indexing process of regular and intermittent impact behaviors because it evaluates the consistency of each impact pattern in multiple impact cycles, as follows:

$$Z_i^* = \frac{p_i}{n}, \quad i = 1, 2, 3, 4 \tag{2}$$

where the subscript i represents an impact surface, p_i is number of impacts registered in a given impact surface evaluated in a determined number of impact cycles, which is represented by the variable n.

Implementing this dynamic parameter results in three major scenarios for each impact surface: a regular impact behavior with an average of one impact per cycle ($Z^* = 1$), an intermittent behavior ($0 < Z^* < 1$), and a scenario without impacts ($Z^* = 0$). This work proposes the analysis of the relation between each Z^* calculated for each impact surfaces to map the different dynamic behavior of this system. The simulations reveals that this dynamic label is associated with two impact surfaces, impact #1 and impact #2. Out of the nine possible combinations, the simulation results reveal that only six different dynamic behaviors were observed, as summarized in Tab. 1.

In this analysis, for each mud flow rate, a set of 200 impact cycles were evaluated after the response achieves steady-state behavior. The relation between the dynamic behavior and the excitation frequency was investigated by observing the

Impact Surface	1st Impact Scenario	2nd Impact Scenario	3rd Impact Scenario	4th Impact Scenario	5th Impact Scenario	6th Impact Scenario
Surface #1	$Z^* = 1$	$0 < Z^* < 1$	$0 < Z^* < 1$	$Z^* = 0$	$Z^* = 0$	$Z^* = 1$
Surface #2	$Z^* = 1$	$Z^* = 1$	$0 < Z^* < 1$	$0 < Z^* < 1$	$Z^* = 1$	$0 < Z^* < 1$

Table 1: Description of each dynamic behavior with their respective impact pattern.

average impact per cycle (Z^*) for each impact surface, as shown in Fig. 3a. These results are compared with the axial vibration peaks to comprehend the effects of the dynamic behavior in the axial acceleration dispersion pattern (see Fig. 3b). Thus, this analysis divides the acceleration peaks in five different impact scenarios; indicating five unique dynamic behaviors (see Tab. 1).

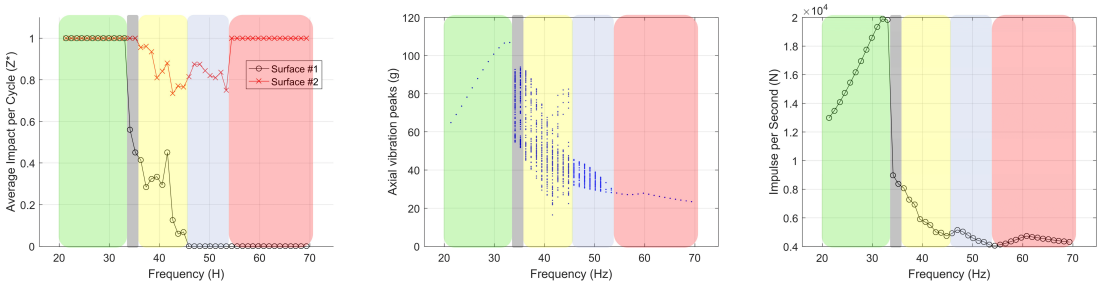

(a) (b) (c)

Figure 3: Simulation results of (a) the dynamic label Z^* associated with their respective impact force scenarios for the impact surfaces #1 and #2, (b) the axial vibration peaks, and (c) impulse per second and their associated impact force scenarios in a flow sweep analysis at an excitation frequency range from 21.3 to 69.3 Hz.

The simulation results shown in Fig. 3 indicate that the first impact force scenario, represented by the green color, is associated with the region having high-average axial acceleration peaks and low-vibration peaks dispersion. In this impact force scenario, there is a direct relation between the increase of the mud flow rate and the increase of the axial vibration peaks. The next region, which corresponds to the second impact scenario (black color), and shows an increase in the axial vibration peaks dispersion when compared with the previous scenario. Furthermore, the following two regions that represent the third (yellow color) and the fourth (blue color) impact force scenarios also present a high axial vibration peak dispersion. The final scenario corresponds to the fifth impact force scenario (red color), which shows relatively low-axial vibration peak dispersion when compared to the other impact force scenarios. Thus, the increase in axial vibration peaks dispersion appears to be related the impact force scenarios that exhibit intermittent impact behavior on at least one impact surface. This observation is further supported by the fact that the first and fifth impact scenarios, which are the only scenarios that do not present intermittent impacts, show low-axial vibration peak dispersion.

3.2 Performance analysis

To evaluate and compare the performance of these impact behaviors (or dynamic labels), an additional parameter is proposed. This parameter is defined as a time average of the impulse, named impulse per second (J^*), as follows:

$$J^* = \frac{1}{\Delta t} \int_{t_0}^{t_1} F dt \tag{3}$$

where J^* is the impulse per second, and F is the impact force applied in the time interval $[t_0, t_1]$.

This dynamic parameter allows the quantification of the performance of the tool because the time normalization enables a reliable and repeatable comparative analysis at different impact frequencies. The analysis of the impulse per second with respect to the mud flow rate (see Fig. 3c) indicates that such dispersion in axial acceleration peaks decreases the performance of the prototype. Further analysis reveals that the first impact force scenario (green color) contains the highest impulse per second when compared with the other impact force scenarios. Therefore, this analysis indicates that the best conditions for operating the tool is within the first impact force scenario, which coincides with the region that exhibits periodic behavior. As a result, the parametric analysis will be focused on this first impact force scenario.

4. PARAMETRIC ANALYSIS

Each parametric analysis focuses on evaluating the behavior of the model, and its performance as each parameter is varied individually. The three parameters selected for this analysis are the recoil spring stiffness, the gap between the

impacting mass and the recoil spring, and the excitation force magnitude.

The analysis of the dynamic behavior of the system uses a nonlinear tool that enables the visualization of the different impact scenarios in a 2D map, as presented by Aguiar and Weber (2011). This map provides information about the characteristics of the impact force (impact scenarios) as a function of a given parameter and the mud flow rate as shown in Fig. 4a. The color scheme used in this map is the same as discussed previously for the impact scenarios (see Tab. 1). Although this map provides valuable information about the impact condition, this map does not provide information regarding the performance of the tool. To overcome this problem, a slight variance of this map is suggested, which exchanges the dynamic label (Z^*) for the impulse per second as the mapped variable as shown in Fig. 4b. In this map variation, only he first impact scenario scenario is addressed because it contains the highest impulse per second values.

The analysis of the mapping of the excitation force magnitude shown in Fig 4a indicates five impact behavior scenarios. In reference to the first impact scenario (green zone), the increase in the excitation force magnitude results in a significant expansion of the frequency range (34 Hz at 300.5 N/kg to 39 Hz at 534.17 N/kg). In reference to the impulse per second, the results shown in of Fig. 4b indicate that when comparing the current design (black line) with the most excellent scenario obtained in this map, there is a 56% increase in impulse per second (from 20 to 31.2 kN) as the excitation force magnitude increases 78% (from 300.5 to 534.17 N/kg). With the available results from the parametric analysis, the selection of the recommended design considers the best performance scenario in each of the parametric analysis. Therefore, the proposed improved design includes 472.4 kN/kg.m of recoil spring stiffness, a 50% increase in the gap between impacting mass and recoil spring, and 534.17-N/kg of excitation force. Furthermore, a performance comparison (impulse per second) between the recommended design and the original prototype is shown in Fig. 4c. The results showed an increase in the impulse per second from 20 to 37 kN, which translates to an 85% increase from the original design.

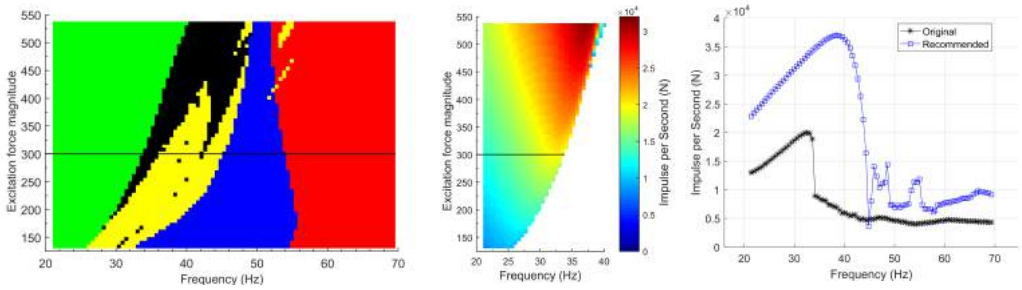

(a) (b) (c)

Figure 4: (a) Impact force scenario mapping and (b) impulse per second distribution within first impact force scenario obtained through parametric analysis of the excitation force magnitude, and (c) simulation results of the impulses per second at an excitation frequency range from 21.3 to 69.3 Hz for the original and the recommended design.

5. CONCLUDING REMARKS

The axial nonlinear dynamics of a vibro-impact system, used as a drilling tool, is analyzed. In this work, the relation between the average impacts per cycle (Z^*) for each impact surface is used to index and map the dynamic behavior observed in the simulation results. Additionally, a performance parameter, named impulse per second (J^*), is proposed to quantify the tool's performance. This parameter accounts for the average force being transmitted from the impacting mass into the bit assembly; therefore, to the rock formation. With the available results from the parametric analysis, the recommended designs shows an 85% increase in performance when compared with the original design.

6. ACKNOWLEDGEMENTS

The authors would like to acknowledge Schlumberger management for authorizing the publication of this article. The third author would like to acknowledge that this study was financed in part by the *Coordenação de Aperfeiçoamento de Pessoal de Nível Superior* (CAPES) - Finance code 001 - Grant PROEX 803/2018, and the Brazilian agencies: *Conselho Nacional de Desenvolvimento Científico e Tecnológico* (CNPQ) - Grants 303302/2015-1, 400933/2016-0, *Fundação Carlos Chagas Filho de Amparo à Pesquisa do Estado do Rio de Janeiro* (FAPERJ) - Grant E-26/201.572/2014.

7. REFERENCES

Aguiar, R. and Weber, H., 2011. "Mathematical modeling and experimental investigation of an embedded vibro-impact system". *Nonlinear Dynamics*, Vol. 65, No. 3, pp. 317–334.

d'Almeida, E., Aguiar, R. and Ritto, T., 2019. "Mathematical model and validation of the axial dynamics of a vibration-assisted drilling tool". In *XVIII International Symposium on Dynamic Problems of Mechanics*.